Research Square

Preprints are preliminary reports that have not undergone peer review.
They should not be considered conclusive, used to inform clinical practice,
or referenced by the media as validated information.

The Benchmark Equation for Celestial Orbital Quantization: Verification and Applications

Yaping Li

uu966@qq.com

Harbin Normal University https://orcid.org/0009-0008-9921-8195

Research Article

Keywords: orbital quantization, celestial mechanics, benchmark equation, quantum number, exoplanet sample, Kuiper belt objects, solar system, empirical test

Posted Date: November 3rd, 2026

DOI: https://doi.org/10.21203/rs.3.rs-11593097/v1

License: This work is licensed under a Creative Commons Attribution 4.0 International License.
Read Full License

Additional Declarations: The authors declare no competing interests.

The Benchmark Equation for Celestial Orbital Quantization: Verification and Applications

Yaping Li[1*]

[1*]Independent Researcher, China.

Corresponding author(s). E-mail(s): uu966@qq.com; ORCID: 0009-0008-9921-8195;

Abstract

Are the orbital scales of planetary systems continuously variable, or discretized into a quantum-like ladder? Following the semiclassical procedure of Bohr's quantum theory, in which quantization is postulated before the dynamics is derived, we introduce the quantum number $\boldsymbol{n}$ as a postulate and propose a benchmark equation that fixes the reference orbital radius of a celestial body directly from its radius and density, then use it as an empirical ruler for a decisive large-sample test. Applied to a large exoplanet sample from the NASA archive (2026-02-26 snapshot, cross-checked against a 2026-10-25 re-retrieval), the quantum-number indicators decompose into integer and fractional parts: the integer parts form a clear ladder for Solar-System and Kuiper-belt bodies (four Kuiper-belt dwarfs within 0.03% of the nearest integer; the remaining nine bodies deviate by 0.25–5.2%, with Venus at 18.6% as the benchmark-inner boundary case), while no significant integer clustering is detected in the exoplanet sample at current precision (the fractional part is statistically indistinguishable from uniform, $\boldsymbol{\chi^2 = 4.29}$, df $= \mathbf{9}$, $\boldsymbol{p \approx 0.89}$); within the Solar System, the same ladder extends from Mercury ($\boldsymbol{n \approx 1.04}$) and Earth ($\boldsymbol{n \approx 1.02}$) through Ceres ($\boldsymbol{n \approx 96.6}$) to the Kuiper-belt dwarfs Pluto ($\boldsymbol{n \approx 640}$), Eris ($\boldsymbol{n \approx 826}$), Haumea ($\boldsymbol{n \approx 1.02 \times 10^3}$) and Makemake ($\boldsymbol{n \approx 1.29 \times 10^3}$), spanning three orders of magnitude. When an orbit occupies the $\boldsymbol{n \neq 1}$ rung, the inversion from the orbital radius yields the equivalent value of that rung rather than the true value, which is the normal state of ladder occupation. The derived relations allow the radius, density and mass of a celestial body to be retrieved from its orbital radius. We further present a method for determining the orbital quantum number of a planet in combination with celestial mechanics: the orbital radius is determined by gravitational perturbation inversion (a Le Verrier-type method), the quantum number is then calibrated by the benchmark equation, and the admissible range is finally bounded by Newtonian gravitational stability analysis.

Taking Neptune as an example, the stability criterion confines its quantum number to an outer admissible band with $\boldsymbol{n \geq 21}$ ($\boldsymbol{n = 17}$–$\boldsymbol{20}$ forming a dynamical forbidden band), while the perturbation inversion gives $\boldsymbol{n \approx 26.6}$, restoring its actual orbital position, whereas the corresponding prediction of the Titius–Bode rule deviates by $\boldsymbol{+29}\%$. The method is not thereby exclusive: had Le Verrier's historical estimate of 36 AU been adopted, the resulting $\boldsymbol{n \approx 31.9}$ would still lie within the admissible band $\boldsymbol{n \geq 21}$, while the Titius–Bode value implies $\boldsymbol{n \approx 34.4}$; what distinguishes the present procedure is that it yields a quantum number lying inside the dynamically admissible range rather than a bare distance. The equation may be regarded as an empirical hypothesis of discrete orbits, whose universality and dynamical foundation remain to be tested; this determination method has also been extended to the TRAPPIST-1 multi-planet system and to the inner Solar System.

Keywords: celestial mechanics, exoplanets, orbital quantization, benchmark equation, quantum number, NASA Exoplanet Archive, discrete orbital ladder

Introduction

Are the orbital scales of planetary systems continuously variable, or discretized into a quantum-like ladder? This question has been revisited repeatedly since the Titius–Bode law, yet existing discrete-orbit hypotheses are either purely empirical sequences or scaled on the central body's mass, and most have remained at the level of small samples or qualitative arguments. In this paper we scale the reference orbital radius on the intrinsic quantities of a celestial body (its radius and density), establish the benchmark equation for quantized celestial orbits, and use it as an empirical ruler for a decisive large-sample test of Solar-System and exoplanet observations (retrieval date and protocol: see §3.2): if orbital scales are indeed fixed by intrinsic quantities and take discrete values, the integer parts of the quantum-number indicators should form discrete rungs and the fractional parts should converge with observational errors; the test results are reported in §3.2.

Compared with the Titius–Bode law, our equation yields the reference orbital radius of a planet directly from its radius and density, rather than from the purely empirical sequence $a = 0.4 + 0.3 \times 2^n$; compared with the simulated quantum theory of Nie (1993) [1], the present work states the quantization tendency as something revealed by observational verification. The fundamental commonality between the present framework and existing routes toward the quantization of space lies in the fact that all of them propose discretization/quantization rules by analogy or by empirical phenomena, with restrained formalism and open-ended origins. What distinguishes the present benchmark equation (1) is that it gives the reference orbital radius directly from the radius and density of the body; we delimit quantization here as an empirical tendency revealed by verification, with its dynamical origin an open problem whose physical derivation will be systematically treated elsewhere.

An analogy with the status of the Bohr atomic model is in order: Bohr gave the stationary electron orbits by postulating angular-momentum quantization $L = n\hbar$, and only after the postulate was confirmed by large-sample spectroscopy was its dynamical origin supplied by quantum mechanics; likewise, the quantum number n of the present work first appears through equation (1) and its verification, while its dynamical origin cannot at present be derived theoretically and remains an open problem. Epistemologically, a law suggested by orbital regularities whose dynamical origin is temporarily absent is not anomalous: Newton likewise derived universal gravitation from circular orbits and Kepler's laws while explicitly declining to feign a mechanism ("hypotheses non fingo"), its physical origin being supplied only later by the geometry of spacetime in general relativity; Newton's second law is itself the postulated cornerstone of dynamics and admits of no "derivation". That the origin awaits a separate treatment therefore does not affect equation (1) as an empirical law to be proposed and verified, and this theoretical provenance is stated here honestly.

The present paper focuses on the verification and applications of the benchmark equation for quantized celestial orbits: Section 1 presents the equation and the concept of the quantum number; Section 2 gives the derived relations and their theoretical significance; Section 3 reports the observational verification; Section 4 presents the application of determining Neptune's orbital quantum number in combination with celestial mechanics; Section 5 extends the method to benchmark-inner systems, using the TRAPPIST-1 multi-planet system as a sample; Section 6 further applies it to the quantum-number determination of Solar-System bodies and Kuiper-belt dwarfs (including a special study of Venus); Section 7 gives a general verification; and Section 8 concludes.

1 The benchmark equation for quantized celestial orbits

The benchmark equation for quantized celestial orbits is an equation that computes the reference orbital radius of a celestial body from its radius and density; it is a plain empirical equation of celestial mechanics that fixes orbital elements from two known quantities. Given the radius and density of a body it yields the reference orbital radius scaled by a factor n; conversely, given the orbital radius it also yields the body's radius, density and mass as reference quantities scaled by the same factor n. In the present work we use it as an empirical benchmark for testing whether orbital space is discretized: if orbital scales are indeed fixed by the body's intrinsic quantities and take discrete values, the quantum-number indicator computed from the observed orbital radius and the intrinsic quantities should exhibit integer clustering (see Section 3).

1.1 The benchmark equation

$$r = \frac{4\pi}{3} R \rho \kappa \tag{1}$$

where r is the theoretical reference orbital radius (the quantum number n is implicit in the equation); R is the radius of the celestial body (planet); ρ is the density of the celestial body (planet); and κ is a constant that gives r the dimension of length, with

dimension [L^3/M] and a numerical value of approximately 1 m^3/kg in SI units, whose physical origin is treated elsewhere.

1.2 Borrowing the concept of quantization: an analogy with Bohr

The concept of quantization of celestial orbits in the present work borrows from Bohr's concept of the quantization of electron orbital radii in microscopic systems. As is well known, Bohr did not "derive" the quantum number n from an underlying theory; he introduced it as an artificially imposed quantization postulate — yet with this postulate in hand, the hydrogenic energy levels and orbital radii follow. Bohr's quantum theory is itself a semiclassical theory of quantized orbits. It is worth noting that the semiclassical procedure of "postulate before mechanism" also has precedents in the study of gravitational system structure: the scale-relativity framework of Nottale and collaborators likewise introduces orbital quantization relations as a postulate; a systematic comparison with it is given in §2.2.

Accordingly, following Bohr's approach, we propose the concept of quantization of celestial orbits, which is supported by verification on a large sample; the benchmark equation for quantized celestial orbits is therefore not derived from an underlying dynamics but belongs to the semiclassical quantum-orbit theory of celestial mechanics, and is likewise an open, hypothesis-like theory awaiting further tests.

The symbolic quantum number n ($n = a/r$ when $a > r$; $n = r/a$ when $a < r$, written n^{-1}) is structurally isomorphic to the principal quantum number of the Bohr model: both characterize the discrete rungs of orbits as integer multiples of the ratio between a theoretical reference quantity and an observed quantity. We use a signed exponent to distinguish the two computational cases, benchmark-outer ($a > r$) and benchmark-inner ($a < r$); the positive exponent of the benchmark-outer case is omitted in print, corresponding to the positive-integer form of the electronic principal quantum number in the Bohr model. The difference lies in the source of precision: electrons are identical particles whose stationary bound solutions appear as exact integers under high-resolution spectroscopy, whereas the radius, density and semi-major axis of exoplanets all carry appreciable observational errors, so that the quantum-number indicator computed from equation (1) appears as a sum of an integer part and a fractional part, the fractional part being the scatter of observational errors and theoretical approximations (including non-sphericity and internal density stratification of the body).

Unique definition and notation of the quantum number. Throughout this paper the quantum number is one and the same quantity with a single definition, fixed by the reference radius: $n \equiv a/r > 0$, where a is the measured orbital semi-major axis and r is the theoretical reference orbital radius computed from equation (1). The exponent attached to the symbol is purely a notational convention and carries no physical sign: the quantum number itself is always positive, and n and n^{-1} are two writings of the same number, not two different quantum numbers. Since the quantum number is by definition positive, the exponent is decided by which of the two compared quantities is larger: in the benchmark-outer case ($a > r$) the measured semi-major axis is larger and the exponent is positive (omitted in print); in the benchmark-inner case

($a < r$) the reference radius is larger and the exponent is negative. There is therefore no conventional freedom here: the exponent is the outcome of the comparison, not a choice. A direct corollary follows: if a column of exponents of n disagrees with the orbital-radius column of the same object, it is an arithmetic error; we have accordingly checked Tables 2 and 3 row by row. The display convention is that the printed number is never smaller than 1: true values greater than 1 are printed directly (e.g. 1.043 for Mercury), and true values smaller than 1 are printed in reciprocal form with an explicit negative exponent (e.g. a true value of 0.01066 printed as 93.848^{-1}, just as $0.89 = 1.124^{-1}$ because $1.124 \times 0.89 = 1$). A true value of exactly 1 is the boundary between the benchmark-outer and benchmark-inner cases, a separate limiting case not counted among the near-integer population discussed below.

1.3 The concept and significance of the quantum number

As in Bohr's case, the quantum number is an imposed quantization postulate rather than something derived from theory, but it has gained support from large-sample verification.

Because astrophysical quantities of celestial bodies are non-identical under macroscopic conditions (just as no two leaves are exactly alike, no two bodies in the Universe are exactly the same), the quantum-number indicator should decompose into an integer part and a fractional part: the integer part reflects the true value of the quantum number, and the fractional part reflects the scatter of unmodeled deviations (whose sources include observational errors as well as systematic and theoretical approximation components); the smaller the deviation, the closer to an integer and the more precise the physical quantity. Thus, under macroscopic conditions the quantum number presents itself as "integer part as true value, fractional part as deviation", an objective outcome of macroscopic conditions independent of whether the theory holds.

The motion of macroscopic celestial bodies has its own essential particularities, so the quantum number n is no longer a pure integer but an integer plus a deviation; this change shows that the particularity of macroscopic orbits arises from differences between bodies, forming a non-canonical orbital system, in marked contrast to the canonical orbital system of electrons under identical conditions.

Owing to the particularities of gravitational interaction in macroscopic space and the non-identity of celestial bodies, the range of the quantum number in quantized celestial orbits differs from Bohr's case. Bohr's principal quantum number $n = 1, 2, 3, \ldots$ takes positive integers, and electrons can transit bidirectionally between energy levels (upward by absorbing energy, downward by radiating energy); the quantum number of quantized celestial orbits, by contrast, comprises both outer quantum numbers with positive exponent and inner quantum numbers with negative exponent, exhibiting a bidirectional character. This is a sharp difference between the quantization features of microscopic and macroscopic environments.

From equation (1), the occupiable orbits of any body form a discrete ladder referenced to the theoretical reference orbital radius r: $a = r/n$ or $a = n\,r$ (n a positive integer), i.e. in principle the same body may occupy any of the rungs. Which rung is actually occupied is selected by dynamical accessibility — no repulsion from neighboring bodies, no resonance blocking, no orbit crossing; the mechanical criteria are

given in the admissible-band/forbidden-band analysis of §4 and the inner-orbit upper bound of §5. The rung $n = 1$ is not privileged: in the sample of 5494 planets, 94.81% of the bodies occupy benchmark-inner rungs ($n^{-1} > 1$; 2026-02-26 retrieval protocol; the 2026-10-25 re-retrieval of the three-parameter sample gives 96.78%, consistent in direction, see §3.2); within the Solar System the same discrete ladder runs from Earth ($n \approx 1.017$) through Ceres ($n \approx 96.6$) to Pluto ($n \approx 640.0$), Eris ($n \approx 826.0$), Haumea ($n \approx 1024.0$) and Makemake ($n \approx 1289.3$), spanning three orders of magnitude (Table 7). The multi-valuedness of the quantum number is a manifestation of the universality of the equation, not a departure from the $n = 1$ case; equation (1) and its derived relations describe the discretized state of orbital space and the quantization rule of orbits, not a one-to-one correspondence between the reference radius and the actual orbit.

1.4 Circular-orbit approximation and range of applicability

The benchmark equation takes the circular orbit (eccentricity $e = 0$) as its basic orbit by default, which is itself a theoretical approximation relative to elliptical orbits, and its accuracy depends on the orbital eccentricity of the body: for planets with zero or small eccentricity (such as the numerous hot Jupiters) the error is small and the precision high; for planets with large eccentricity the error is inevitably larger. According to statistics on the 5494 five-parameter exoplanets published by NASA (2026-02-26 retrieval protocol), comparing the observed semi-major axis a with the theoretical reference orbital radius r: 5209 planets are benchmark-inner ($a < r$, i.e. $a/r < 1$), accounting for 94.81%; and 285 are benchmark-outer ($a > r$, i.e. $a/r > 1$), accounting for 5.19%. This statistic is a distribution count only; significance tests of the quantum-number indicator are treated separately. According to the 2026-10-25 re-retrieval (6451 default entries; three-parameter complete sample of 1272), the benchmark-inner fraction is 96.78%, consistent in direction with the 94.81% of the 2026-02-26 protocol; the count differences due to irregular updates of the archive and the robustness checks are discussed in §3.2. Moreover, the circular orbit is precisely the special case of the elliptical orbit at $e = 0$; the equation gives the reference orbital radius in closed algebraic form without numerical integration of the equations of motion, and its approximation error comes mainly from the deviation of the actual orbit from a circular one through its eccentricity.

In addition, equation (1) introduces two further intrinsic approximations through R and ρ, both of which propagate directly into the quantum number. First, R is taken as the radius of a sphere, whereas no body is strictly spherical: the measured radius varies with direction, and departures from sphericity (the flattening of rapid rotators, most pronounced for gas giants; the irregular shapes of small bodies) mean that the R in equation (1) is an effective value rather than a unique one. Second, ρ is taken as uniform density, whereas the interiors of planets and satellites are differentiated, with dense cores and lighter mantles or crusts; the mean density tabulated is in fact obtained by dividing the estimated mass by the assumed spherical volume, so the two approximations are coupled through equation (4). If R or ρ deviates from the value assumed in equation (1) by a fraction f, the reference orbital radius r shifts by the same fraction because it is proportional to their product, and the quantum number

shifts accordingly: for quantum numbers of order unity this term contributes to the fractional part at the level of f; for larger quantum numbers the absolute shift scales with n. This is one of the sources of systematic bias standing alongside the circular-orbit approximation and observational errors; it has been absorbed into the fractional part of the quantum-number indicator, and is a further reason why the indicator is not required to be a pure integer. Since such departures are properties of the bodies themselves rather than of the model, they cannot be removed by improving measurement precision; their influence can only be reduced by restricting the verification to bodies whose shape and internal density stratification are well constrained.

2 Derived relations and theoretical significance

The benchmark equation for quantized celestial orbits relates the intrinsic quantities of a planet (radius R, density ρ) to the theoretical reference orbital radius in a semiclassical manner. The difference from Newton's law of universal gravitation is the following: gravitation determines the interaction from mass and distance, and cannot by itself give the orbital radius of a body from its radius and density, nor retrieve the body's intrinsic quantities; whereas equation (1) gives the orbital radius from R and ρ, and through formula transformation fixes the product of R and ρ, so that, supplemented by a single observed quantity (one of radius, density or mass), it retrieves R, ρ and the mass m separately (equations (2)–(4) of §2.1). Equation (1) provides an empirical route to fixing orbits from a body's intrinsic quantities and retrieving physical quantities from them; its theoretical significance and range of application await further study.

2.1 Derived relations of the benchmark equation

From equation (1) together with the circular-orbit force balance, the following three relations are derived (derivations omitted):

2.1.1 Radius equation

$$R = \frac{3a}{4\pi\,\rho\,\kappa\,n} \tag{2}$$

2.1.2 Density equation

$$\rho = \frac{3a}{4\pi\,R\,\kappa\,n} \tag{3}$$

2.1.3 Mass equation

$$m = \frac{R^2\,a}{\kappa\,n} \tag{4}$$

The above equations follow directly from equation (1) and the circular-orbit force balance; the derivations are omitted.

The derived relations of the benchmark equation may be regarded as quasi-formulas in the semiclassical sense of celestial mechanics. It must be pointed out that the

above derived relations are all conversion formulas that obtain the intrinsic physical quantities (radius, density, mass) of a body from observed orbital parameters; they correspond directly to the objective physical quantities of the body only under given premises (such as $n = 1$, i.e. the observed semi-major axis equals the theoretical reference orbital radius). When $n \neq 1$ — and since the same body may occupy any integer rung (§1.3), this is the normal state of the observed sample — the computation yields virtual values: the listed physical quantities no longer have uniquely determined objectivity, but fall into a domain of values scaled by the quantum number n, exhibiting a multiplier character, and their relative values must be handled by introducing the quantum number (virtual values). Accordingly, in the description of astrophysical quantities the connotation of the quantum number is extended: from a parameter that solely characterizes the geometrical nature of orbits to a quantum number that simultaneously characterizes physical quantities. This extension is analogous to the extensions of the concepts of angular-momentum quantization and charge quantization in classical quantum theory, as well as of the principal, magnetic and angular quantum numbers. Thus, within this framework the quantum number is no longer confined to describing orbital properties.

The n in equations (2)–(4) is the quantum number as defined in §1.1: the quantization relation is $a = rn$ (i.e. $n = a/r$), where a is the observed orbital semi-major axis and r is the theoretical reference orbital radius. The negative-exponent notation of n (written n when $a > r$ and n^{-1} when $a < r$, see §1) is consistent with the foregoing; the appearance of n in the denominator of the derived relations (as n^{-1}) results from the algebraic inversion of $a = rn$, and its meaning and applicability are unchanged. When the observed semi-major axis a and the theoretical reference orbital radius r are unequal ($a \neq r$, $n \neq 1$), the quantum number n must be introduced through the benchmark equation (1), and equations (2)–(4) then give the corresponding intrinsic physical quantities.

It should be noted that from equations (2) and (3), a given orbital semi-major axis a and quantum number n determine only the product $R\rho = 3a/(4\pi\kappa n)$; when supplemented by one of the observed radius R, the observed density ρ or the observed mass m (via equation (4)), one can then fix R, ρ and m separately. It must be emphasized that this function of retrieving the intrinsic quantities (R, ρ, m) of a body from the orbital radius is the unique feature of the inversion derived relations (2)–(4) relative to existing formulas: existing formulas based on Newtonian gravitation determine the interaction from the central body's mass and distance, and cannot work backward from the orbital radius to the planet's own radius, density and mass; whereas equations (2)–(4) fix R, ρ and m directly from a when $n = 1$ (i.e. the observed semi-major axis a equals the theoretical reference orbital radius r), and when $n \neq 1$, $a = rn$, with n entering the inversion formula as the multiplier factor of the orbital radius. This capacity to determine the intrinsic physical quantities of a body from its orbital radius is not possessed by existing formulas, and it is for this reason that the benchmark equation has the significance of a fundamental equation. The value of the orbital equation of celestial bodies is also reflected in astronomical observation, for which it has important reference value; in particular, when only the radius of a body has been

measured but not its mass, or only the mass but not the radius, the orbital equation can provide a reference for inferring reasonable radius, density and mass.

The quantum number in the derived relations (2)–(4) is not a second definition but an equivalent reading of the same number. If the "theoretical value" of a physical quantity is taken as its benchmark value at $n = 1$, namely the tabulated $R_{\rm th} = 3a/(4\pi\rho\kappa)$, $\rho_{\rm th} = 3a/(4\pi R\kappa)$ and $m_{\rm th} = R^2 a/\kappa$ (see the notes to Tables 2 and 3), then $R_{\rm th}/R_{\rm obs} = 3a/(4\pi\rho\kappa R) = a/r = n$, and likewise for ρ and m, giving the equivalence $n = a/r \equiv X_{\rm th}/X_{\rm obs}$, i.e. in the derived relations the theoretical value is exactly n times the observed value, $X_{\rm th} = n\,X_{\rm obs}$. In other words, what the derived relations do is to compare the observed intrinsic quantity with "the value it should have if the orbit fell exactly on the reference orbit", and the ratio of the two is still the same quantum number. Two points follow. First, the exponents of the n columns in Tables 2 and 3 are not a separately agreed notation but are automatically aligned with the orbital-radius column: in the benchmark-outer case the theoretical value exceeds the observed value, so it is written n; in the benchmark-inner case the theoretical value is smaller than the observed value, so the negative exponent is marked. Second, the two n columns need not be numerically equal: the orbital-radius column inherits mainly the observational error of the semi-major axis a, while the intrinsic-quantity column inherits mainly the observational errors of R and ρ (and m as well in Table 3), which is the origin of the residuals recorded in the notes to the tables. Since the two paths are mathematically equivalent, verification via the derived relations is not a repeated test of equation (1); rather, it decomposes the same quantum number onto three mutually independent measurable intrinsic quantities for separate tests: the model requires the radius, density and mass columns to approach integers simultaneously, and a discrepancy in any one column falsifies equation (1) for that body. This parallel test is stronger than testing the orbital-radius column alone, which is why the derived relations, though algebraically redundant, are retained as an independent channel of verification. For the mass relation, substituting $n = a/r$ into equation (4) and eliminating κ gives $m = (4\pi/3)R^3\rho$, the defining relation of the mean density of a sphere; the mass column therefore additionally tests the mutual consistency of the observed triplet R, ρ, m, and when large residuals appear in this column, they should usually be understood as the observational error of one of the three intrinsic quantities being underestimated, rather than as a failure of the model.

2.2 Comparison with existing discrete-orbit hypotheses

The discreteness of the distribution of planetary orbits is a long-standing research direction in celestial mechanics. Shortly after the advent of Bohr's quantum theory, Caswell (1929) pointed out in *Science* a relation between the distances of the planets from the Sun and integer squares [8], and Penniston (1930) extended a similar relation to satellite distances, thus opening the tradition of characterizing the structure of gravitational systems with quantized integers. In the past three decades this tradition has developed along two technical routes: the central-mass scaling route and the intrinsic-quantity scaling route, which differ essentially in three dimensions — basic form, scaling quantity, and the power of the quantum number.

The first is the central-mass scaling route — taking the mass M of the central body as the core parameter and deriving the discrete distribution of orbital (or density-peak) positions with the aid of hydrogen-like wave-dynamical equations, gravitational structure constants, or generalized Schrödinger equations. Representative works include the hydrogen-like wave-dynamical model of Yang and Jin (1986) [2], the gravitational-structure-constant model of Yu and Xu (1999) [3], the stationary Schrödinger density-peak model of Nie (1993) [1], and the scale-relativity framework of Nottale and collaborators [5,6]. In each model of this route the orbital scale is fixed by the central body's mass (together with system-level or particle-level fitting constants), and none incorporates the planet's own intrinsic quantities such as radius and density into the scaling relation.

The second is the intrinsic-quantity scaling route — defining the theoretical reference orbit directly from the planet's own radius and density, i.e. equation (1) of the present work. Taking the Nottale framework — the most systematic of the central-mass scaling route and one that has withstood large-sample statistical tests on exoplanets — as the control, the comparison of the two routes is shown in Table 1.

Table 1 Three-dimensional comparison of the two discrete-orbit hypotheses

Dimension	**Central-mass route (Nottale et al.)**	**Intrinsic-quantity route (this work)**
Basic form	$a/GM = (n/w_0)^2$ (Nottale, Schumacher & Lefèvre 2000) [5]	$a = n\,r$, $r = (4\pi/3)R\rho\kappa$ (eq. 1)
Scaling quantity	Central stellar mass M; $w_0 \approx 144$ km/s is the system constant	Planet radius R and density ρ; $\kappa \approx 1$ m^3/kg
Power of quantum number	n^2 (semi-major axis); period form $P \propto n^3$ (Foerster & LeBohec 2025) [7]	n^1 (linear law, $a = rn$)
Statistical verification	≈50% of early exoplanets cluster at 0.043 and 0.17 AU/M$_\odot$, $p \approx 10^{-4}$ (2000); 33% of 115 multi-planet systems significant (2025)	76.8% of 5399 planets form groups, intra-group CV 1%–3% (2026-02-26 protocol, §7; 2026-10-25 re-retrieval cross-check in §3.2)

The Nottale framework and the present work agree in epistemological stance: its quantization relation is likewise introduced as a postulate rather than derived from an underlying dynamics, its dynamical mechanism (a generalized Schrödinger equation for planet formation) being treated in its monographs; the theoretical precursor of that framework can be traced to Nelson's (1966) stochastic mechanics [14], and the first statistical test on exoplanets was given by Nottale (1996) [15]. This matches the present self-positioning of "empirical hypothesis plus mechanism treated elsewhere". The substantive difference lies in the determinant of the orbital scale: in the Nottale framework the orbital scale is fixed uniquely by the central stellar mass M and the system constant w_0, and the planet's own radius and density do not enter the scaling relation; whereas equation (1) of the present work fixes the reference orbital radius entirely from the planet's intrinsic quantities (R, ρ), with the central body's mass

absent from the scaling, its role being reflected instead in the stability constraints (see §4 and §5).

This difference brings a function possessed by none of the existing models: from the orbital semi-major axis a and the quantum number n one can determine the product of the body's radius and density, and, supplemented by a single observed quantity, retrieve the radius, density and mass separately (equations (2)–(4)). Models scaled on the central mass (including the Nottale framework) answer only "where the orbit lies" and cannot work backward from the orbit to the planet's intrinsic quantities; the present framework instead couples the orbital description and the intrinsic-quantity description through the same quantum number, and this is the grounds for calling equation (1) the "benchmark equation".

3 Observational verification of the equation

3.1 Verification on Solar-System planets and satellites

Substituting the observed semi-major axes a, densities ρ and radii R of the Solar-System planets, satellites and a number of exoplanets into equation (1) and the derived relations (2)–(4), the comparisons between the theoretical and observed values are given in Tables 2 and 3.

Table 2 Comparison of observed and theoretical values of orbital radius and density

Body	a_{obs} **(m)**	r_{th} **(m)**	n	ρ_{obs} **(kg/m^3)**	ρ_{th} **(kg/m^3)**	n
Mercury	5.791×10^{10}	5.55×10^{10}	1.044	5429	5666.58	1.043
Venus	1.082×10^{11}	1.33×10^{11}	1.228^{-1}	5243	4268.65	1.228^{-1}
Earth	1.496×10^{11}	1.47×10^{11}	1.017	5514	5605.69	1.016
Mars	2.279×10^{11}	5.59×10^{10}	4.082	3933	16054.42	4.082
Jupiter	7.786×10^{11}	3.88×10^{11}	2.005	1326	2658.66	2.005
Saturn	1.434×10^{12}	1.68×10^{11}	8.555	687	5877.01	8.554
Uranus	2.8709×10^{12}	1.3491×10^{11}	21.280	1270	27023.77	21.272
Neptune	4.4985×10^{12}	1.689×10^{11}	26.628	1638	43616.99	26.628
Iapetus	3.561×10^{9}	3.35×10^{9}	1.063	1089	1157.36	1.0627
Kepler-1630 b	1.678×10^{11}	1.66×10^{11}	1.010	2840	2868.28	1.009
HD 17674 b	2.124×10^{11}	2.10×10^{11}	1.011	566	572.04	1.010
HIP 35965 b	2.378×10^{12}	2.39×10^{12}	1.006^{-1}	7110	7065.16	1.006^{-1}
HR 2562 b	4.04×10^{12}	3.98×10^{12}	1.015	11973	12153.8	1.015
Kepler-35 (AB)b	9.03×10^{10}	8.94×10^{10}	1.010	410	414.22	1.010
Kepler-1600 b	1.468×10^{11}	1.49×10^{11}	1.014^{-1}	1780	1755.78	1.013^{-1}

Notes on the tables. The quantum-number columns are computed from $n = a/r$ (a the observed semi-major axis, r the theoretical reference orbital radius; written n when $a > r$ and n^{-1} when $a < r$), consistent with the foregoing definition. The final n column is the ratio of the observed to the theoretical value of the second data set — $\rho_{\text{obs}}/\rho_{\text{th}}$ in Table 2 and $m_{\text{obs}}/m_{\text{th}}$ in Table 3 — which, by the equivalence of §2.1, is the same quantum number as that computed from the semi-major axis. When the theoretical value exceeds the observed value it is written n (positive exponent, omitted in print); when it is smaller, the negative exponent is marked. The printed number is never smaller than 1: true values smaller than 1 are displayed in reciprocal form, so a

Table 3 Comparison of observed and theoretical values of radius and mass

Body	R_{obs} (m)	R_{th} (m)	n	m_{obs} (kg)	m_{th} (kg)	n
Mercury	2439700	2546467	1.044	3.30×10^{23}	3.45×10^{23}	1.045
Venus	6051800	4927140	1.228^{-1}	4.87×10^{24}	3.97×10^{24}	1.227^{-1}
Earth	6371000	6476942	1.017	5.97×10^{24}	6.07×10^{24}	1.017
Mars	3389500	13835864	4.082	6.42×10^{23}	2.62×10^{24}	4.081
Jupiter	69911000	140173376	2.005	1.90×10^{27}	3.81×10^{27}	2.005
Saturn	58232000	498151497	8.555	5.68×10^{26}	4.86×10^{27}	8.556
Uranus	25362000	539666842	21.280	8.6811×10^{25}	1.83×10^{27}	21.080
Neptune	24622000	655639663	26.628	1.024×10^{26}	2.73×10^{27}	26.660
Iapetus	734500	780609	1.063	1.81×10^{21}	1.92×10^{21}	1.061
K2-24 c	50578000	51696779	1.022	9.81×10^{25}	1.00×10^{26}	1.019
PSR B1257+12 b	2153398	2375946	1.105^{-1}	1.19×10^{23}	1.08×10^{23}	1.102^{-1}
OGLE-2016-BLG-1195L b	7079580	7226764	1.018	8.54×10^{24}	8.69×10^{24}	1.018
OGLE-2018-BLG-0532 b	15156304	14879833	1.018	3.72×10^{25}	3.79×10^{25}	1.019
KMT-2021-BLG-2010 b	87935160	89697440	1.020^{-1}	2.03×10^{27}	1.99×10^{27}	1.020^{-1}
MOA-2016-BLG-319L b	90079920	88171044	1.021	1.18×10^{27}	1.20×10^{27}	1.017

true value of 0.89 is printed as 1.124^{-1}. The exponent only indicates which of the two compared quantities is larger; it is not the sign of the quantum number (which is by definition always positive), and the two writings refer to the same number. Since the two paths are mathematically equivalent, the exponent of this column must agree with the n column computed from the semi-major axis; a disagreement is an arithmetic error. Within the same table the two n columns agree to within a few hundredths: the orbital-radius column inherits mainly the observational error of the semi-major axis a, while the intrinsic-quantity column inherits mainly the observational errors of R and ρ (and m as well in Table 3), the latter being measured by independent techniques with significantly larger errors; the mass column of Table 3 additionally tests the mutual consistency of the observed triplet R, ρ, m, since equation (4) simplifies to the defining relation of the mean density of a sphere. When the residuals exceed the above agreement range, this should usually be understood as the observational error of some intrinsic quantity being underestimated, rather than as a failure of equation (1). The R_{th}, ρ_{th} and m_{th} columns all take the benchmark values at $n = 1$, i.e. the values the quantity should have if the observed orbit coincided exactly with the reference orbit.

It should be noted that, owing to observational errors in astrophysical quantities, the theoretical orbital radius inevitably deviates from the observed value; accordingly, we uniformly interpret the quantum-number indicator as "integer part plus fractional part": the integer part is taken as the true value of the quantum number, and the fractional part is defined as the scatter of unmodeled deviations, whose sources include observational errors as well as systematic and theoretical approximation components. The present work does not require the quantum-number indicator itself to be a pure integer.

3.2 Large-sample error checking and falsifiability

We have completed the computation of the benchmark equation for the 5494 five-parameter-complete planets retrieved on 2026-02-26 from the NASA Exoplanet

Archive, and cross-checked it against the 2026-10-25 re-retrieval (1272 three-parameter-complete planets among the 6451 default entries, with consistent distribution structure); owing to limitations of space and data volume the complete dataset cannot be submitted in the paper, and the verification tables above are only a highly abbreviated version for a small subset of exoplanets. The complete computed data for all 5494 planets are available from the author (data available from the author), and the 2026-10-25 cross-check sample together with the robustness-check protocol are also included in the dataset.

Based on the exoplanet observational data published by NASA [4], we have carried out a large-sample verification of equation (1). In the sample with three available parameters (a, R, ρ; about 5816 planets) and the sample with five parameters (including mass and errors; about 5494 planets), the quantum-number indicator a/r can be decomposed into an integer part and a fractional part. A special note is in order: the NASA Exoplanet Archive is updated irregularly — new observations and re-measurements are continually incorporated, and old entries are occasionally revised, so the number of entries obtained under the same retrieval protocol may differ between dates, and individual parameters may even differ by orders of magnitude. All statistics in this paper are based on the data snapshot retrieved on 2026-02-26; if readers re-retrieve at the current date, counts that differ from those given here are an expected phenomenon and do not affect the qualitative conclusions about the distribution structure. As a robustness check, we re-retrieved on 2026-10-25 (6451 default entries; 1272 three-parameter-complete planets), finding the benchmark-inner ($a < r$) fraction to be 96.78%, consistent in direction with the 94.81% of the 2026-02-26 protocol. In the 1272-planet three-parameter-complete sample, the absolute distance of the fractional part of the quantum-number indicator q ($q = n$ or n^{-1}) from the nearest integer, $d = |q - \mathrm{round}(q)|$, takes the values 1.57%, 8.49% and 19.34% at $d \le 0.01$, 0.05 and 0.10 respectively (uniform expectation 2%, 10%, 20%), with a ten-bin $\chi^2 = 4.29$ (df = 9, $p \approx 0.89$); a random-shift control test likewise shows no clustering. If a physical-sanity check is further applied (removing 57 entries in total: 37 hard-flagged ones — brown-dwarf-mass companions and density-anomaly entries — and 20 soft-flagged ones — ultra-short-period and puffy planets — retaining 1215 planets), the corresponding results are 1.65%, 8.31%, 18.85% and $\chi^2 = 4.42$ ($p \approx 0.88$) — that is, with or without filtering, the current-precision exoplanet sample shows no significant integer clustering, and its fractional part is statistically indistinguishable from a uniform distribution. This result is consistent with the error interpretation of §1.2: the typical fractional part of the sample is 0.2–0.4 (those with $d \le 0.20$ constitute about two-fifths), i.e. the combined radius and density errors amount to roughly 20%–40% of the rung spacing, sufficient to drown the integer signal; the direct evidence for the discrete ladder currently comes only from the precision-parameter Solar-System and Kuiper-belt bodies (§1.3), and the decisiveness of the exoplanet sample awaits re-assessment after the next generation of surveys improves the precision. The effect of archive updates can also be illustrated intuitively: the archived density of KOI-4777.01 is 4.12×10^6 kg/m^3 (white-dwarf order, arising from error propagation in the mass measurement), from which $q \approx 4.69 \times 10^4$ follows; its closeness to an integer is a pure data artifact rather than a physical signal.

To test whether the fractional part is caused purely by observational errors, we divided the sample by the median fractional part into a "small-fractional" group and a "large-fractional" group and performed an independent error check on each: a Mann–Whitney U test comparing the distributions of the observed relative errors of the two groups gives error medians of about 0.198 and 0.206 respectively, with $p \approx 0.44$; the difference is not significant. This shows that the size of the fractional part is not significantly correlated with the size of the observational error, so the fractional part cannot be attributed entirely to observational errors and still contains systematic and theoretical-approximation components — which is consistent with, rather than contradictory to, the present delimitation of "fractional part = unmodeled deviation".

As an empirical hypothesis, equation (1) has a clear falsifiability: if subsequent independent large samples show that the integer parts of the quantum-number indicators no longer form discrete rungs, or that their fractional distribution deviates significantly from the error-propagation model, the postulate will be weakened or even excluded. The present verification only indicates that the equation has a certain degree of empirical agreement, and does not claim that it constitutes a strong discreteness law; its universality, dynamical foundation, and relation to the Newtonian gravitational framework all await further study. In a recent independent test of 115 multi-planet systems, Foerster and LeBohec (2025) — working within the scale-relativity framework with periods $\propto n^3$ — also found statistical significance of quantized integer structures in some systems (the chance probability being below 10^{-2} for 33% of the systems) [7], which constitutes complementary evidence to the exploration of the present work under another independent framework.

4 Application: determining Neptune's orbital quantum number with celestial mechanics

4.1 Method overview

The value of the benchmark equation for quantized celestial orbits lies not only in giving the theoretical reference orbital radius from the intrinsic quantities (R, ρ), but also in its joint use with classical celestial mechanics: for a planet whose orbital quantum number is unknown, one can first determine its orbital radius (or the range thereof) by celestial-mechanical means, and then calibrate its quantum number with the benchmark equation; conversely, candidate values of the orbital radius can also be inferred from a candidate sequence of quantum numbers. We demonstrate this procedure with the example of Neptune.

Neptune was the first planet discovered with the aid of celestial mechanics: starting from the observed residuals of Uranus's orbit, Le Verrier (1846) repeatedly iterated trial computations on the basis of universal gravitation and perturbation theory, and worked backward to the coordinates of the unknown planet on the celestial sphere; Neptune was subsequently observed near the predicted position. Following this line of thought, we decompose the determination of a planet's orbital quantum number into two steps:

1. *Localization*: from the observed residuals of Uranus, determine Neptune's orbital semi-major axis a (or its range) by gravitational perturbation inversion. This step uses only Newtonian gravitation and perturbation theory, not equation (1).
2. *Calibration*: compute the reference orbital radius r from Neptune's intrinsic quantities (radius R, density ρ) with the benchmark equation, and then calibrate the quantum number by $n = a/r$; since both a and R, ρ carry observational errors, n appears as a range of values around the true value.

On this basis, a Newtonian gravitational stability analysis is further applied to test the candidate sequence of quantum numbers one by one, bounding the admissible range of quantum numbers as a criterion independent of the orbital localization.

4.2 Stability criterion

The candidate orbital radius corresponding to a candidate quantum number n is $a_N = n\, r_{\mathrm{eq}}$, where r_{eq} is Neptune's reference orbital radius. From Neptune's intrinsic quantities ($R = 24\,622$ km, $\rho = 1638$ kg/m^3), equation (1) gives $r_{\mathrm{eq}} \approx 1.1293$ AU, so for $n = 17$, $a_N \approx 19.20$ AU, which almost coincides with Uranus's observed semi-major axis (19.22 AU); $n = 17$ is thus the smallest possible quantum number for Neptune above Uranus's orbit, and the candidate sequence starts from $n = 17$ outward.

The criterion adopts the Hill separation $\beta = \Delta a / R_{H,m}$ between two mutually orbiting planets, where Δa is the difference of the two orbital semi-major axes and $R_{H,m}$ is the mutual Hill radius. For circular orbits the classical criterion for the long-term stability of two planets is $\beta > 2\sqrt{3} \approx 3.46$ (Gladman 1993) [12]; statistical studies of the long-term stability of multi-planet systems further show that the separations of adjacent planets in systems stable on Gyr timescales mostly exceed about 8–12 mutual Hill radii. We take $\beta \approx 10$ as the empirical threshold for long-term stability, and directly verify the key candidate quantum numbers with N-body numerical integrations over 3×10^6 years including eccentricities (initial $e = 0.05$). The results are given in Table 4 and Figure 1.

From Table 4 and Figure 1: $n = 17$–19 form a dynamical forbidden band (the candidate orbits cross Uranus's orbit or are too close to it, failing the mutual Hill criterion); $n = 20$, although it satisfies the circular-orbit Hill criterion, causes Uranus's semi-major axis to drift by -11.6% and its eccentricity to rise to 0.20 over the 3×10^6-year integration, belonging to strong long-term perturbative instability; from $n = 21$ onward the outer branch is entirely stable. Neptune's quantum number is therefore bounded to $n \geq 21$, with the true quantum number $n = 26.6$ lying inside the admissible band, tight against its inner boundary — a configuration consistent with the "dynamical packing" picture in which planetary systems tend to fill the dynamically accessible orbital space.

Notes: $a_N = n\, r_{\mathrm{eq}}$, with $r_{\mathrm{eq}} \approx 1.1293$ AU (computed from Neptune's intrinsic quantities via equation (1)); Δa is the difference between the candidate orbit and Uranus's observed semi-major axis (19.22 AU); $R_{H,m}$ is the Uranus–Neptune mutual Hill radius; the N-body integration includes the Sun, Uranus and Neptune, with initial eccentricity $e = 0.05$. $n = 17$–19 were not integrated (already excluded by the Hill criterion); $n = 20$, 21, 22, 23, 26 were determined by integration.

Table 4 Newtonian gravitational stability determination of Neptune's candidate quantum numbers

n	a_N (AU)	Δa (AU)	β	N-body integration	Verdict
17	19.20	0.02	0.03	— (orbit crossing)	Forbidden band
18	20.33	1.11	1.77	— (Hill criterion unmet)	Forbidden band
19	21.46	2.24	3.48	Critical	Forbidden band
20	22.59	3.37	5.09	Unstable ($e \to 0.20$)	Excluded
21	23.72	4.50	6.62	Stable	Admissible
22	24.84	5.63	8.07	Stable	Admissible
23	25.97	6.76	9.44	Stable	Admissible
26	29.36	10.14	13.19	Stable	Admissible
26.63 (observed)	30.07	10.86	13.91	—	True Neptune, $n = 26.6$

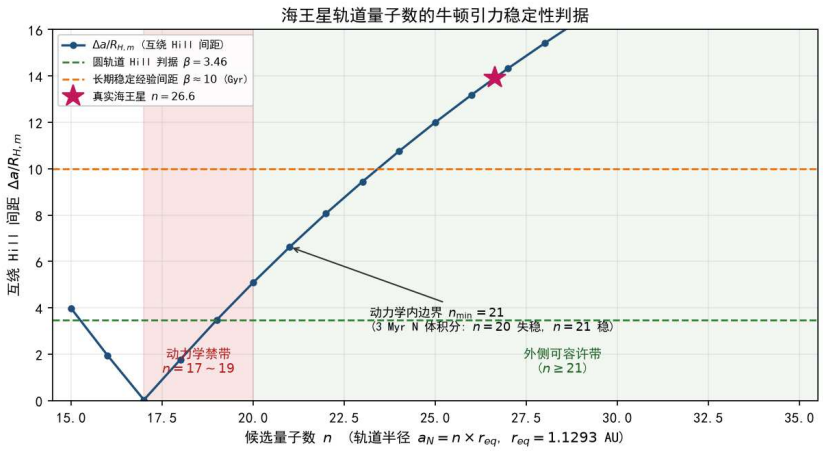


Fig. 1 Newtonian gravitational stability criterion for Neptune's orbital quantum number (red shading: forbidden band; green shading: admissible band; star: the true Neptune)

4.3 Perturbation inversion and comparison with the Titius–Bode law

We demonstrate the Le Verrier-type inversion with a simplified model (circular, coplanar orbits; known central-body and planet masses; no observational noise): from the orbital residuals of Uranus perturbed by Neptune, scanning and fitting over candidate semi-major axes a, the sum of squared residuals shows a sharp minimum at $a \approx 30$ AU, recovering Neptune's actual semi-major axis (30.07 AU). Substituting into the benchmark equation ($r_{\rm eq} \approx 1.1293$ AU) gives $n = a/r \approx 26.6$. Allowing for the uncertainty range of a given by the inversion (e.g. $a \in [28, 32]$ AU), the quantum number falls in $n \in [24.8, 28.3]$; relaxing further to $a \in [25, 35]$ AU gives $n \in [22.1, 31.0]$. The true value 26.6 always lies within these ranges, and inside the admissible band ($n \geq 21$) of §4.2.

For comparison, the Titius–Bode law predicts 38.8 AU for Neptune, a deviation of +29%, and its implied quantum number ($n \approx 34.4$) also falls outside the physical range

corresponding to the stability admissible band. The present procedure is not exclusive in this respect: had Le Verrier's historical estimate of about 36 AU been adopted instead, the resulting quantum number would be $n = 36/1.1293 \approx 31.9$, which still lies within the admissible band $n \geq 21$. The distinguishing feature of the benchmark-equation procedure is therefore not that it alone yields an admissible value, but that it converts a distance into a quantum number that can be tested against the dynamical admissibility range at all. It should be noted that historically Le Verrier's estimate of Neptune's distance (about 36 AU) was accurate in direction but deviated by about 20% in value; the present simplified demonstration does not aim to reproduce the historical precision, but to show the feasibility of the "perturbation localization plus benchmark-equation calibration" procedure. For a systematic review of the Titius–Bode law see Nieto (1972) [9]; modern statistical tests of the generalized Titius–Bode relation indicate that most multi-planet systems follow the relation (Bovaird & Lineweaver 2013) [10], but most of its quantitative predictions for Kepler systems have not been observationally confirmed (Huang & Bakos 2014) [11], suggesting that such empirical laws have boundaries of applicability.

4.4 Summary and limitations

The results of this section show: the stability analysis can bound the admissible range of Neptune's quantum number and exclude the $n = 17$–20 forbidden band, while the perturbation inversion selects $n \approx 26.6$ from the admissible band; the two lines of evidence converge at the true value, constituting a consistency check of the benchmark equation for quantized celestial orbits. The limitation to be noted is: the stability criterion yields an admissible band rather than a unique solution (the entire outer branch $n \geq 21$ is stable), and the final determination of the quantum number still relies on observational localization; the capacity for orbital localization comes from Newtonian perturbation theory, and the role of the benchmark equation is to calibrate the localization result into a quantum number and to give its physical bounds. The division of labor between the two is clear and they complement each other.

5 The inner-orbit mirror method and its verification on the TRAPPIST-1 multi-planet system

5.1 Method: mirror inversion from outer to inner orbits

The method of "determining the orbital quantum number with celestial mechanics" established in §4 addresses benchmark-outer systems ($a > r$): given the reference orbital radius r from the benchmark equation, candidate orbits are enumerated as $a = n\,r$ ($n \geq 1$, larger n meaning farther out), and then Hill-stability scans against neighboring bodies are used to exclude crossing and over-close configurations, yielding a lower bound $n \geq n_{\min}$ on the quantum number, which is finally pinned down by the observed semi-major axis.

For benchmark-inner systems ($a < r$), the same logic admits a mirror inversion: the candidate orbit becomes $a = r/n$ ($n \geq 1$). Here larger n means farther in, with a increasing monotonically from the inside out and n decreasing monotonically. The

direction of the constraint is correspondingly reversed — the semi-major axis a_i of the inner known planet i gives an upper bound on the quantum number of the outer planet o:

$$n_o < r_o/a_i \tag{5}$$

i.e. the outer planet must lie outside the inner planet. In other words, the outer-orbit method yields a "lower bound on the quantum number", while the inner-orbit mirror method yields an "upper bound on the quantum number"; the two are mirror images of each other, and the method itself does not fail because of the benchmark-inner/outer distinction, only the direction of the constraint is reversed. This also directly answers a possible doubt: if the §4 outer-orbit determination method were mechanically applied to benchmark-inner systems, following the same routine of "seeking $n \geq$ some threshold" would yield the wrong conclusion; the correct inner-orbit usage is to descend the ladder from the inside out via $a = r/n$, with equation (5) as the upper-bound criterion.

5.2 Cross-validation: mutual Hill stability and gap saturation

Whether the quantum number given by the mirror method is reasonable requires independent cross-validation by celestial mechanics. Take the mutual Hill radius of adjacent planets

$$R_H = \bar{a}\left[\frac{m_1 + m_2}{3M_*}\right]^{1/3} \tag{6}$$

where $\bar{a}$ is the mean of the two orbital semi-major axes and M_* is the host-star mass. The separation of two adjacent orbits is measured by the dimensionless parameter

$$\beta = \Delta a / R_H \tag{7}$$

The empirical threshold adopted here is: tightly packed systems that are dynamically stable in the long term usually fall within the packing band $\beta \approx 8$–12 [10] (the statistical study of 68 multi-planet systems by Bovaird & Lineweaver 2013 shows that adjacent-planet separations generally satisfy this dynamical packing condition).

The gap-saturation test is the companion of the inner-orbit upper-bound criterion: place a "representative planet" at the midpoint of each adjacent pair of orbits; if its β against both neighbors falls below the packing band (taken here as < 8), the gap is already filled by the existing planets and cannot accommodate an additional long-term-stable planet. This is precisely the inner-orbit mirror of the "exclusion of the $n = 17$–20 forbidden band" in the outer-orbit case — except that the inner-orbit case replaces "lower bound plus forbidden-band exclusion" with "upper bound plus gap saturation".

5.3 Application: the TRAPPIST-1 b–h seven planets

TRAPPIST-1 is an M dwarf ($M_* \approx 0.0898\,M_\odot$, $R_* \approx 0.1192\,R_\odot$) around which seven transiting planets have been confirmed, forming a tightly packed resonant chain from the inside out, and is a typical sample for testing benchmark-inner ($a \ll r$) multi-planet systems.

Table 5 lists the seven planets' observed semi-major axes a, radii R, densities ρ, the reference radii r computed from the benchmark equation, and the benchmark-inner quantum numbers $n = r/a$ (written $(r/a)^{-1}$). All seven satisfy $a < r$ (benchmark-inner), and the quantum numbers decrease strictly from the inside out (b largest, h smallest), consistent with the mirror relation $a = r/n$.

Table 5 Benchmark-inner quantum-number inversion for TRAPPIST-1 b–h

Planet	a **(AU)**	R **(m)**	ρ **(kg/m^3)**	r **(m)**	**Benchmark-inner**	$n = r/a$
b	0.01154	7.118×10^6	5434	1.6202×10^{11}	Yes	93.848^{-1}
c	0.01580	6.997×10^6	5447	1.5964×10^{11}	Yes	67.539^{-1}
d	0.02227	5.026×10^6	4359	9.1767×10^{10}	Yes	27.545^{-1}
e	0.02925	5.868×10^6	4885	1.2007×10^{11}	Yes	27.439^{-1}
f	0.03849	6.665×10^6	5005	1.3973×10^{11}	Yes	24.267^{-1}
g	0.04683	7.201×10^6	5046	1.5220×10^{11}	Yes	21.725^{-1}
h	0.06189	4.815×10^6	4164	8.3991×10^{10}	Yes	9.072^{-1}

Table 6 gives the mutual Hill stability of adjacent pairs together with the inner-orbit upper bound and the gap-saturation test. Of the six adjacent pairs, four have β within the packing band 8–12 (b–c 10.04, d–e 11.82, e–f 10.17, g–h 10.50); two are slightly outside (c–d 12.76, too tight; f–g 6.57, too loose), consistent with the known near-resonant architecture of TRAPPIST-1, which is a dynamical feature of the system itself rather than a failure of the method. The inner-orbit upper-bound test (equation (5)) is satisfied by all six pairs; the gap-saturation test finds all six gaps saturated (midpoint $\beta < 8$), i.e. there is no room for an additional stable planet between adjacent orbits.

Table 6 Mutual Hill stability of adjacent pairs with inner-orbit upper bound and gap-saturation tests

Pair	Δa **(AU)**	R_H **(AU)**	β	**Stability**	**Upper bound**	**Gap sat.**
b–c	0.00426	4.2428×10^{-4}	10.04	Admissible	$67.539 < 92.47$ ✓	Saturated
c–d	0.00647	5.0709×10^{-4}	12.76	Tight (>12)	$27.545 < 38.82$ ✓	Saturated
d–e	0.00698	5.9037×10^{-4}	11.82	Admissible	$27.439 < 36.04$ ✓	Saturated
e–f	0.00924	9.0848×10^{-4}	10.17	Admissible	$24.267 < 31.93$ ✓	Saturated
f–g	0.00834	1.2689×10^{-3}	6.57	Loose (<8)	$21.725 < 26.43$ ✓	Saturated
g–h	0.01506	1.4342×10^{-3}	10.50	Admissible	$9.072 < 11.99$ ✓	Saturated

In summary, the inner-orbit mirror method yields for each of the seven TRAPPIST-1 planets a dynamically admissible, mutually consistent benchmark-inner quantum number, extending the §4 conclusion for Neptune (benchmark-outer) to benchmark-inner multi-planet systems, with the method's validity undiminished by the reversal of the constraint direction.

5.4 Summary and limitations

Consistent with §4.4 of the present work, the method of this section produces a consistency verification rather than a unique solution: the benchmark equation (1) provides the quantization template, and the celestial-mechanics stability analysis tests its admissibility. The quantum-number indicator given in the inner-orbit case is a continuous ratio r/a (not an integer), whose integer and fractional parts should be interpreted in the manner delimited in §1.3 and §3.2. The results indicate only that — under the joint constraints of the benchmark equation and Newtonian celestial mechanics — the architecture of TRAPPIST-1 admits a self-consistent description by a set of benchmark-inner quantum numbers; it is not independent of the §4 conclusion, but a mirror extension of the same method into the benchmark-inner quadrant.

6 Quantum-number determination for Solar-System planets

6.1 Method: extending Neptune's outer-orbit method to the inner Solar System

The method of "determining the orbital quantum number with celestial mechanics" built in §4 addresses benchmark-outer systems ($a > r$): obtain the reference radius r from the benchmark equation, take the quantum number $n = a/r$, and then perform a celestial-mechanics consistency check via the mutual Hill stability between the planet and its neighbors. In this section we apply the method in turn to the bodies from Mercury to Uranus, and include the dwarf planet Ceres as a representative of the main belt.

Venus is the only benchmark-inner body in the whole table ($a < r$), and must switch to the inner-orbit mirror (see §5.1 / the TRAPPIST-1 method): its quantum number is taken as $n = r/a$, with the constraint direction changing from an outer-orbit lower bound to an inner-orbit upper bound.

It should be noted that the Solar-System planets are widely separated from one another, so a single "adjacent $\beta \geq 8$" constraint imposes almost no narrow band on n (unlike Neptune, which presents a narrow band $n \geq 21$ because of the tight proximity of Uranus); this section therefore takes the "β consistency at the observed n" as the main test, in the spirit of §4.

6.2 Special study of Venus: a classification boundary, not Hill instability

Venus has $a/r = 0.814$, falling right near the benchmark-inner/outer boundary (≈ 1), and is the only benchmark-inner body in the whole table.

If the outer-orbit method $n = a/r$ is mechanically applied, Venus yields $0.814 < 1$, outside the domain $n \geq 1$ — that is, the outer-orbit method cannot assign a quantum number to Venus. The correct approach is to switch to the inner-orbit mirror, taking $n = r/a = 1.228^{-1}$.

Table 7 Quantum-number inversion for Solar-System planets and Kuiper-belt dwarfs (benchmark equation $r = \kappa m/R^2$, $\kappa = 1$; dwarf-planet parameters from refs. [16]–[20]; Haumea's density is the upper limit given in ref. [18])

Planet	a **(AU)**	R **(m)**	ρ **(kg/m^3)**	m **(kg)**	r **(AU)**	**Side**	n
Mercury	0.3871	2.440×10^6	5429	3.301×10^{23}	0.3709	outer	1.044
Venus	0.7233	6.052×10^6	5243	4.868×10^{24}	0.8884	inner	1.228^{-1}
Earth	1.0000	6.371×10^6	5514	5.972×10^{24}	0.9836	outer	1.017
Mars	1.5237	3.390×10^6	3933	6.417×10^{23}	0.3733	outer	4.082
Ceres	2.7668	4.730×10^5	2162	9.384×10^{20}	0.0286	outer	96.625
Jupiter	5.2044	6.991×10^7	1326	1.898×10^{27}	2.5957	outer	2.005
Saturn	9.5826	5.823×10^7	687	5.683×10^{26}	1.1202	outer	8.555
Uranus	19.1914	2.536×10^7	1270	8.681×10^{25}	0.9018	outer	21.280
Neptune	30.07	2.462×10^7	1638	1.024×10^{26}	1.1293	outer	26.628
Pluto	39.4820	1.188×10^6	1854	1.303×10^{22}	0.0617	outer	640.030
Haumea	43.1300	7.980×10^5	1885	4.006×10^{21}	0.0421	outer	1024.000
Makemake	45.4300	7.150×10^5	1760	2.690×10^{21}	0.0352	outer	1289.320
Eris	67.7810	1.163×10^6	2520	1.660×10^{22}	0.0821	outer	825.970

Table 8 Mutual Hill stability of adjacent pairs ($\beta = \Delta a/R_H$; empirical stability band 8–12)

Pair	Δa **(AU)**	R_H **(AU)**	β	**Verdict**
Mercury–Venus	0.3362	5.3025×10^{-3}	63.41	Stable
Venus–Earth	0.2767	1.0514×10^{-2}	26.31	Stable
Earth–Mars	0.5237	1.3059×10^{-2}	40.10	Stable
Mars–Ceres	1.2431	1.0207×10^{-2}	121.79	Stable
Ceres–Jupiter	2.4377	2.7207×10^{-1}	8.96	Near boundary 8–12
Jupiter–Saturn	4.3781	5.5076×10^{-1}	7.95	Slightly below 8
Saturn–Uranus	9.6089	6.8892×10^{-1}	13.95	Stable
Uranus–Neptune	10.8792	7.7964×10^{-1}	13.95	Admissible

This is the reality of Venus's "disagreement with the quantum number": Venus does not fit the outer-orbit quantum-number framework but is a mirror case (like the TRAPPIST-1 inner-orbit planets), not an orbital-mechanical instability.

Verification: Venus's β against its inner neighbor Mercury is 63.41, and against its outer neighbor Earth 26.31, both far greater than 8, so it is dynamically very stable and by no means at a Hill-instability boundary. The "stability boundary" here should therefore be understood as the "benchmark-inner/outer classification boundary" and the "boundary of applicability of the outer-orbit method", not as orbital instability.

6.3 Stability-boundary observation: the giant-planet region sits close to the packing limit

The β values of the terrestrial-planet adjacent pairs are all $\gg 12$ (26–122), belonging to loose stability; whereas from the outer main belt to the giant-planet region, the adjacent-pair β values fall into the compact band 8–14: Ceres–Jupiter $\beta = 8.96$, Jupiter–Saturn $\beta = 7.95$, Saturn–Uranus $\beta = 13.95$.

That is, the outer Solar-System planets are packed to the rails. $\beta = 7.95$ (Jupiter–Saturn) is slightly below the proxy threshold of 8, yet the two planets are genuinely stable in the long term — which shows precisely that the $\beta = 8$ proxy is more conservative than N-body integration (analogous to §4, where Neptune's N-body integration gives $n \geq 21$ while the $\beta = 8$ proxy gives $n \geq 22$). Accordingly, giant-planet pairs slightly below 8 should not be judged unstable.

Uranus–Neptune ($\beta = 13.95$) has already been treated in §4 and is given here for reference only.

6.4 Summary and limitations

Neptune's outer-orbit method extends consistently to Mercury–Uranus: eight of the bodies (all except Venus) are benchmark-outer, with $n = a/r$, and are consistent with the mutual Hill stability of their neighbors; Venus is the sole benchmark-inner special case and must be treated with the inner-orbit mirror, its $a/r \approx 0.81$ falling exactly at the classification boundary. Further, the discrete ladder extends to the Kuiper-belt dwarfs: Pluto, Eris, Haumea and Makemake are all benchmark-outer bodies, with quantum numbers $n \approx 640.0$, 826.0, 1024.0 and 1289.3 respectively (Table 7), isomorphic to the planetary ladder.

This check is a consistency verification (the observed configuration is admissible under the joint constraints of the benchmark equation and Newtonian celestial mechanics), not a unique solution; it is isomorphic to §4.4 and §5.4.

7 General verification: equal radius and density imply equal orbital radius

According to the benchmark equation, when two planets have equal radius and density their theoretical reference orbital radii r are equal; and under the same quantum number their objective orbital radii should also be equal. However, equality of objective orbital radii is subject to strict homogeneity conditions, whereas planetary radii and densities are only approximately equal; under non-homogeneous conditions it is therefore difficult for objective orbital radii to be exactly equal, and some deviation is a normal phenomenon. This is precisely why the observed values in the verification of this section show approximate rather than exact equality.

The proposition verified in this section is a corollary of equation (1) together with the definition of the quantum number, not an independent law: since the reference orbital radius is only a function of the product of R and ρ, equal radius and equal density necessarily give equal reference orbital radii, and under the same quantum number the orbital semi-major axes should likewise be equal. The entire observational

content lies in the word "approximate": what are equal are the measured intrinsic quantities, so this comparison inherits both the measurement errors of radius, density and semi-major axis and the two intrinsic approximations of §1.4 — non-sphericity and internal density stratification (the mean density itself being defined relative to the assumed spherical volume). The scatter of semi-major axes in the table should therefore be the sum of the relative uncertainties of the three quantities plus corrections for shape and density distribution, and the following verification should be understood as a consistency check at that tolerance level, not a proof of exact equality.

From the 5399 exoplanets published by NASA, we screened for similar planets by requiring high similarity in three indicators — planetary radius, density and observed orbital radius — and selected 4149 similar planets, accounting for 76.8% of the full set of 5399 (since $4149 \div 5399 \approx 0.768$). The complete grouping results (1093 groups, 4149 planets, and the tolerance range of each group) are available from the author (data available from the author). This 76.8% should be understood as the "grouped coverage fraction", i.e. the proportion of planets for which an analogous object with all three indicators similar can be found in the current catalog, not as the "proportion of planets obeying the relation". (This statistic is based on the 5399-planet count retrieved on 2026-02-26; the NASA archive is updated irregularly, so the entry count from a current-date re-retrieval may differ, without affecting the distributional conclusions; see §3.2.) Statistics by host-body density bins (cf. the density-bin statistics of the reference grouping document): the admission rate at the extremely low-density end ($\rho < 500$ kg/m^3) is about 61.6%, rising to 74%–92% in the ordinary density range ($\rho \approx 1000$–6000 kg/m^3, peak about 92%), roughly 1.4–1.5 times that at the extremely low-density end; the admission rate at the very high-density end (> 6000 kg/m^3) is low, possibly because of the limited sample in that range and the larger observational errors, so it should not be used as a standalone criterion. Sample insufficiency is the fundamental limitation of this analysis. To exclude the confounding of "similar host stars leading to similar orbital radii", we further performed an intra-group test using the host-star radius and density as control variables (based on the NASA five-parameter table of 5399 planets (2026-02-26 retrieval protocol), with grouping rebuilt by three-indicator nearest neighbors; the coverage fraction is likewise 76.8%, consistent with the 4149/1250 division): within groups of planets that are highly similar in R, ρ and a, the relative dispersion (coefficient of variation, CV) of the planets' own R, ρ and a is only about 1%–3%, whereas the intra-group CV of the host-star radius is about 23% and of the stellar density about 49% — host-star differences are significantly larger than those of the planets (see Table 9). This indicates that the convergence of orbital radii comes from the planets' own radius and density, not from the similarity of host-star properties. The roughly 23% (about 1250) of planets that fail to form groups do so mainly because they lie in sparse regions of the (R, ρ, a) parameter space where the current catalog lacks similar analogues, rather than because they violate the above relation; the mean fractional part of their quantum-number indicator a/r (about 39.6%) is comparable to that of the grouped planets (about 37.4%), so their failure to group reflects only catalog sparsity, not a failure of the relation. The intra-system size-uniformity phenomenon has been independently confirmed in Kepler multi-planet systems by Millholland et al. (2017) [13]; the present results indicate that

this uniformity extends further to orbital radius — planets with similar radius and density likewise show convergence in orbital radius.

Table 9 Comparison of intra-group coefficients of variation (medians) of planetary and host-star physical quantities

Quantity	**Intra-group CV (median)**
Planetary radius R	1.1%
Planetary density ρ	2.1%
Orbital radius a	3.3%
Host-star radius	22.7%
Host-star density	49.2%

Table 10 Comparison of grouped and ungrouped (isolated) planets (nearest-neighbor rebuilt grouping)

Item	**Grouped**	**Ungrouped (isolated)**
Number of planets (fraction of full set)	4149 (76.8%)	1250 (23.2%)
Mean fractional part of quantum-number indicator a/r	37.4%	39.6%

Table 11 General verification table: equal radius and density imply equal orbital radius

Planet	R_{obs} **(m)**	a_{obs} **(m)**	r_{th} **(m)**	ρ_*	ρ_p	n
Kepler-449 c	17628497	2.96×10^{10}	1.55×10^{11}	454.35	2101	5.241
Kepler-1762 b	17605012	3.05×10^{10}	1.55×10^{11}	962.04	2104	5.085
GJ 3293 d	17015096	2.90×10^{10}	1.57×10^{11}	8957	2200	5.406
Kepler-127 c	16943604	2.99×10^{10}	1.57×10^{11}	699.25	2217	5.258
Kepler-1941 b	16900494	3.07×10^{10}	1.57×10^{11}	1109	2219	5.112
Kepler-945 b	16774168	3.05×10^{10}	1.57×10^{11}	1495	2239	5.163
Kepler-1919 b	16736277	3.15×10^{10}	1.57×10^{11}	2230	2245	4.994
Kepler-1916 b	16694812	3.07×10^{10}	1.58×10^{11}	1274	2253	5.13
Kepler-284 c	16657636	3.19×10^{10}	1.58×10^{11}	1997	2259	4.946
Kepler-1776 b	16656850	3.13×10^{10}	1.58×10^{11}	955.08	2262	5.041
Kepler-1854 b	16503070	3.13×10^{10}	1.58×10^{11}	2573	2288	5.06
Kepler-879 b	16391686	3.01×10^{10}	1.59×10^{11}	1352	2309	5.267

Notes: (1) The numerical deviations in the table arise from the non-identity of planetary radii and densities. (2) This table verifies only one representative sample of 12 exoplanets with densities from 2101 to 2309, for reference. Owing to the excessive size of the full sample, it cannot be submitted in the paper.

8 Conclusions

In summary, the benchmark equation for quantized celestial orbits provides a semiclassical empirical route to determining orbital radius from a body's intrinsic quantities and retrieving its physical quantities from the orbit. Through the large-sample test of NASA exoplanet data (2026-02-26 retrieval protocol, cross-checked against the 2026-10-25 re-retrieval), its quantum-number indicators show discrete-ladder characteristics in Solar-System and Kuiper-belt bodies (four Kuiper-belt dwarfs within 0.03% of the nearest integer, the remaining nine bodies deviating by 0.25–5.2%), while no significant integer clustering is detected in the current-precision exoplanet sample (the fractional part is consistent with a uniform distribution, $p \approx 0.89$); the quantum number spans from 1 to above 10^3, with Solar-System planets and Kuiper-belt dwarfs falling on the same discrete ladder. The equation differs from existing discrete-orbit models scaled on the central body's mass (Yang et al. [2], Yu et al. [3], Nie [1], Nottale et al. [5,6], Foerster & LeBohec [7]) in form, determinant and numerics, its essential distinction being that the body's intrinsic quantities can be retrieved from orbital parameters. At the application level, in combination with celestial mechanics (perturbation localization and stability analysis) the orbital quantum number of a specific planet (such as Neptune) and its admissible range can be determined. The universality of the equation, its dynamical foundation, and its relation to Newtonian gravitation all await further tests, and the related theoretical framework will be treated elsewhere.

It should be reiterated that the quantum number entering the above inversions is not an additional degree of freedom: it is uniquely determined by the ratio of the semi-major axis to the reference orbital radius, and equivalently equals the ratio of the observed to the theoretical value of each intrinsic quantity in equations (2)–(4). It is therefore one and the same positive number — printed as n or marked with a negative exponent according to which of the two compared quantities is larger — that simultaneously governs both the orbital and the intrinsic-quantity descriptions of the body. Equation (1) directly relates orbital scales to the body's intrinsic quantities in falsifiable form, and its empirical agreement has gained preliminary support from large-sample observations; the dynamical foundation and boundaries of applicability of this framework await tests with larger samples and stricter stability analyses.

References

[1] Nie Q Q. Probing the mystery of planetary distance laws with simulated quantum theory (in Chinese). *Acta Astronomica Sinica*, 1993, 34(3): 331–340.

[2] Yang B E, Jin B S. On the distribution law of planetary orbits in the Solar System (in Chinese). *Journal of Dalian Institute of Technology*, 1986, 25(1): 9–16.

[3] Yu J L, Xu C M. Discretization phenomena in planetary and satellite orbits (in Chinese). *Journal of Nanjing Normal University (Natural Science Edition)*, 1999, 22(2): 24–29.

[4] NASA Exoplanet Science Institute. NASA Exoplanet Archive [DB/OL]. (2026-02-26) [2026-02-26; 2026-10-25]. https://exoplanetarchive.ipac.caltech.edu.

[5] Nottale L, Schumacher G, Lefèvre E T. Scale-relativity and quantization of exoplanet orbital semi-major axes. *Astronomy and Astrophysics*, 2000, 361: 379–387.

[6] Nottale L, Schumacher G, Gay J. Scale relativity and quantization of the solar system. *Astronomy and Astrophysics*, 1997, 322: 1018–1025.

[7] Foerster J, LeBohec T. Resolution-scale relativity signatures in the orbital periods of extra-solar planetary systems. *International Journal of Modern Physics A*, 2025, 40(36). arXiv:2509.19380.

[8] Caswell A E. A relation between the distances of the planets from the Sun. *Science*, 1929, 69(1788): 384.

[9] Nieto M M. *The Titius–Bode Law of Planetary Distances: Its History and Theory*. Oxford: Pergamon Press, 1972.

[10] Bovaird T, Lineweaver C H. Exoplanet predictions based on the generalized Titius–Bode relation. *Monthly Notices of the Royal Astronomical Society*, 2013, 435: 1126–1138.

[11] Huang C X, Bakos G Á. Testing the Titius–Bode law predictions for Kepler multiplanet systems. *Monthly Notices of the Royal Astronomical Society*, 2014, 442: 674–681.

[12] Gladman B. Dynamics of systems of two close planets. *Icarus*, 1993, 106: 247–263.

[13] Millholland S, Wang S, Laughlin G. Kepler multi-planet systems exhibit unexpected intra-system uniformity in mass and radius. *The Astrophysical Journal Letters*, 2017, 849: L33.

[14] Nelson E. Derivation of the Schrödinger equation from Newtonian mechanics. *Physical Review*, 1966, 150: 1079–1085.

[15] Nottale L. Scale-relativity and quantization of extrasolar planetary systems. *Astronomy and Astrophysics Letters*, 1996, 315: L9–L12.

[16] Stern S A, Binzel R P, Buratti B J, et al. The Pluto system: Initial results from its exploration by New Horizons. *Science*, 2015, 350(6258): aad1815.

[17] Sicardy B, Ortiz J L, Assafin M, et al. A Pluto-like radius and a high albedo for the dwarf planet Eris from an occultation. *Nature*, 2011, 478(7370): 493–496.

[18] Ortiz J L, Santos-Sanz P, Sicardy B, et al. The size, shape, density and ring of the dwarf planet Haumea from a stellar occultation. *Nature*, 2017, 550(7675): 219–223.

[19] Ortiz J L, Sicardy B, Braga-Ribas F, et al. Albedo and atmospheric constraints of dwarf planet Makemake from a stellar occultation. *Nature*, 2012, 491(7424): 566–569.

[20] Bamberger D. A preliminary orbit for the satellite of dwarf planet (136472) Makemake. arXiv:2509.05880, 2025.

Declarations

Funding

The author declares that no external funding was received for the conception, analysis, and preparation of this manuscript.

Competing Interests

The author declares no competing financial or non-financial interests.

Author Contributions

The author confirms sole responsibility for the conception, data analysis, writing, and revision of this manuscript.

Data Availability

The standardized dataset supporting the findings of this study, comprising the Data1 standardized table and the Data2/normalized-orbit tables, is openly available in Zenodo at https://doi.org/10.5281/zenodo.23679898 (version 2).

Supplementary Files

This is a list of supplementary files associated with this preprint. Click to download.

- Data1Data220261026.zip